

Chain End Mobilities in Polymer Melts – A Computational Study

Diddo Diddens^{1,2,*} and Andreas Heuer^{1,2}

¹*Institut für physikalische Chemie, Westfälische Wilhelms-Universität
Münster, Corrensstrasse 28/30, 48149 Münster, Germany*

²*NRW Graduate School of Chemistry, Corrensstrasse 36, 48149 Münster, Germany*

(Dated: August 16, 2012)

The Rouse model can be regarded as the standard model to describe the dynamics of a short polymer chain under melt conditions. In this contribution, we explicitly check one of the fundamental assumptions of this model, namely that of a uniform friction coefficient for all monomers, on the basis of MD simulation data of a PEO melt. This question immediately arises from the fact that in a real polymer melt the terminal monomers have on average more intermolecular neighbors than the central monomers. The mobilities are determined by our recently developed statistical method¹, which provides complementary information about the local polymer dynamics and thus contrasts standard quantities such as the mean square displacement (MSD) or the Rouse mode analysis. Within our analysis it turned out that the Rouse assumption of a uniform mobility is fulfilled to a good approximation for the PEO melt, although the underlying microscopic dynamics is highly affected by different contributions from intra- and intermolecular excluded volume interactions, which, each in itself, cannot be taken into account by a modified friction coefficient. However, in the sum, these non-trivial terms roughly cancel each other, and the overall dynamics corresponds to that of a phantom chain. These effects remain elusive when studying the dynamics with the MSD only, since this observable characterizes a sum over dynamical contributions due to the bare mobility, chain connectivity and more complicated local potentials.

PACS numbers: 36.20.Ey 61.25.H-

I. INTRODUCTION

The Rouse model^{2,3} is one of the standard models to describe the dynamics in a polymer melt of non-entangled chains. Here, the polymer chain is modeled as a sequence of N harmonically linked beads. All intermolecular interactions of the chain are reduced to a frictional and a stochastic force, both characterized by the friction coefficient ζ via the Fluctuation-Dissipation Theorem³. Within this model, ζ takes the same value for all beads irrespective of the monomer position n . However, when going to real polymer melts, it is obvious that the individual polymer segments along the chain cannot have exactly the same intermolecular environment due to chain connectivity. A terminal segment has on average more intermolecular neighbor segments in its first coordination sphere than a segment located in the center of the chain. Therefore, it is questionable if the assumption of a uniform friction constant along the entire chain as assumed in the Rouse model still holds for a realistic chain in the melt.

The dynamics of the chain ends also plays a special role in the limit of long chains, which is usually described by the reptation model⁴. Within this picture, the topological constraints imposed by the other chains are modeled as a tube³, and the tagged chain performs Rouse-like motion within this effective tube. Here, the local dynamics of the chain ends play an important role in a twofold manner: First, since the chain can only escape the tube at its ends, one would expect that the dynamics of the chain ends significantly influences the overall relaxation mechanism. For example, it has been observed

in simulations^{5–7} that the tube constraints are less pronounced for the terminal monomers. Improved models suggest that the tube relaxation is enhanced by so-called contour-length fluctuations³, which have also been observed experimentally⁸. Here, the motion of the chain ends leads to a loss of memory of the initial tube. Second, switching to the surrounding chains imposing the tube constraint, it was argued that the chain ends do not contribute to the formation of entanglements, and a revised tube model has been proposed^{9,10}. Experimental data of a bimodal melt was successfully interpreted within this concept¹¹, and it was observed that a matrix of shorter chains and thus a higher chain end concentration reduces the effective entanglement formation.

A different but related interplay of topological constraints and the chain end dynamics becomes important if a polymer melt approaches the glass transition temperature T_g . The dependence of the glass transition temperature on the molecular weight is usually described by the empirical Flory-Fox equation¹². Within this picture, the chain ends experience a larger amount of free volume than the central monomers, leading to a lower T_g for short chains. Recently, the characteristic T_g -dependence was also investigated in MD simulations¹³.

In this contribution, we study the dynamics of the chain ends and the central segments in a non-entangled PEO melt significantly above T_g by means of MD simulations. In particular, we check the classical assumption of a uniform friction coefficient as employed in the Rouse model. This is done by applying our recently developed method to determine segmental mobilities from simulation data (pq-method¹). The results for the PEO melt are interpreted within the simpler semiflexible chain

model (SFCM¹⁴), in which a Rouse chain is augmented by an additional angle potential, thus incorporating chain stiffness. From a technical point of view, additional emphasis is put on the comparison of our method with conventional dynamical quantities such as the mean square displacement (MSD). In the course of our analysis, interesting chain end effects are observed, which cannot be captured by a modified friction coefficient, but rather reflect more subtle intra- and interchain interactions.

II. SIMULATION DETAILS

For our analysis, MD simulation data of a PEO melt from a previous study¹⁵ has been used. The system consisted of 16 PEO chains with $N = 48$ monomers each. The simulations were performed in the NVT ensemble with the GROMACS simulation package¹⁶ using an effective two-body polarizable force field¹⁷. The temperature had been maintained at $T = 450$ K by a Nosé-Hoover thermostat.

Additionally, the SFCM¹⁴ has been simulated via Brownian Dynamics (BD) Simulations. In this model, a Rouse chain is augmented by a bending potential of the form

$$U_\theta(\{\mathbf{R}_n\}) = -k_\theta \sum_{n=2}^{N-1} \frac{(\mathbf{R}_{n+1} - \mathbf{R}_n)(\mathbf{R}_n - \mathbf{R}_{n-1})}{|\mathbf{R}_{n+1} - \mathbf{R}_n||\mathbf{R}_n - \mathbf{R}_{n-1}|}, \quad (1)$$

where the \mathbf{R}_n correspond to the position vectors of the beads. Here, the value of $k_\theta/(k_B T) = 2.1$ has been chosen, for which we found that the characteristic ratio of the SFCM matches that of the PEO chains in the MD simulations. Naturally, the semiflexible chains contained the same number of monomers ($N = 48$) as the PEO chains. For the friction coefficient ζ , the temperature $k_B T$ and the mean squared bond length b^2 , unit values were used. In this case, a time-step of $\Delta t = 0.002$ turned out to be sufficiently small in order to propagate the system with a simple Euler integrator.

III. PQ-METHOD

To briefly review the pq-method¹, we start with a stroboscopic view on the local Langevin dynamics of monomer n of a polymer chain

$$\mathbf{p}_n(t, \Delta t) = -A_n(\Delta t)\mathbf{q}_n(t) + \text{noise}, \quad (2)$$

where the definitions

$$\mathbf{p}_n(t, \Delta t) = (1/\Delta t) [\mathbf{R}_n(t + \Delta t) - \mathbf{R}_n(t)] \quad (3)$$

and

$$\mathbf{q}_n(t) = 2\mathbf{R}_n(t) - \mathbf{R}_{n+\Delta n}(t) - \mathbf{R}_{n-\Delta n}(t) \quad (4)$$

have been used. In case of the terminal monomers, eq. 4 can be modified according to $\mathbf{q}_1 = \mathbf{R}_1 - \mathbf{R}_{1+\Delta n}$ and

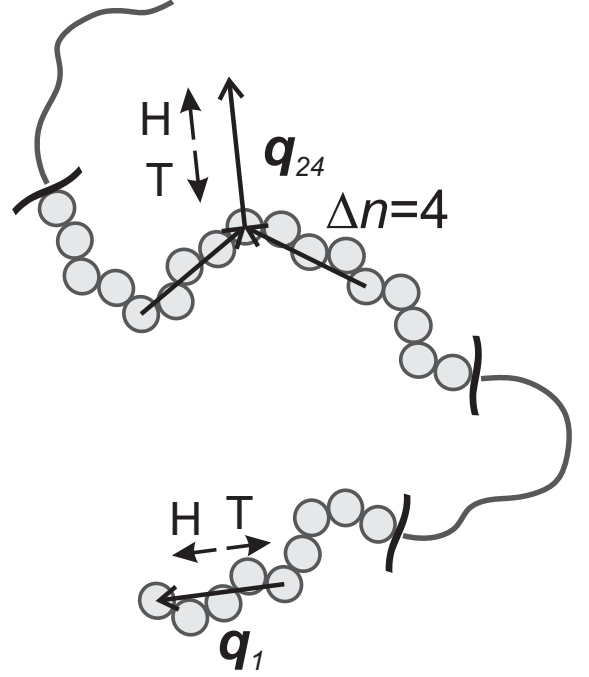


Figure 1: Sketch depicting various definitions used in the present analysis for a simplified excluded volume chain. Depending on the direction in which the center of mass of the subchain consisting of all monomers within \mathbf{q}_n moves during time Δt , one can distinguish between head (H) and tail (T) monomers (see text for further explanation).

$\mathbf{q}_N = \mathbf{R}_N - \mathbf{R}_{N-\Delta n}$ (fig. 1). For polymer chains with a certain stiffness, Δn corresponds to the number of chemical monomers within one Kuhn segment, and was chosen such that $C_\infty \approx [(\langle (\mathbf{R}_n - \mathbf{R}_{n-\Delta n})^2 \rangle / \langle (\mathbf{R}_n - \mathbf{R}_{n-1})^2 \rangle)]^{1/2}$ is approximately fulfilled. The characteristic ratio in turn was determined from the mean squared end-to-end vector $\langle \mathbf{R}_e^2 \rangle$ using the identity $C_\infty = \langle \mathbf{R}_e^2 \rangle / [(N_0 - 1)b_0^2]$, where b_0^2 is the average squared distance between two chemical monomers (in total N_0). For PEO ($C_\infty = 3.2$), $\Delta n = 4$ was obtained. Due to the choice of k_θ in eq. 1, the same Δn -value was used for the SFCM.

Eq. 2 serves as a definition of a time-dependent, effective mobility $A_n(\Delta t)$, which for a Rouse chain with $\Delta n = 1$ approaches the true ratio k/ζ in the limit $\Delta t \rightarrow 0$. Here, $k = 3k_B T/b^2$ is the entropic force constant and b^2 the average squared bond length between two Kuhn segments. For finite Δt and appropriate Δn eq. 2 maps the local dynamics of a more realistic chain (i. e. the SFCM or PEO) onto the Langevin dynamics of a Rouse bead, thus yielding an effective mobility $A_n(\Delta t)$ for bead n on the time scale Δt . From simulation data, $A_n(\Delta t)$ can easily be determined by a linear regression

$$A_n(\Delta t) = \frac{\langle p_{n,\alpha}(\Delta t) q_{n,\alpha} \rangle}{\langle q_{n,\alpha}^2 \rangle} = \frac{\langle \mathbf{p}_n(\Delta t) \mathbf{q}_n \rangle}{\langle \mathbf{q}_n^2 \rangle}, \quad (5)$$

where α represents the Cartesian coordinates and $\langle p_{n,\alpha}(\Delta t) \rangle = \langle q_{n,\alpha} \rangle = 0$ due to isotropy.

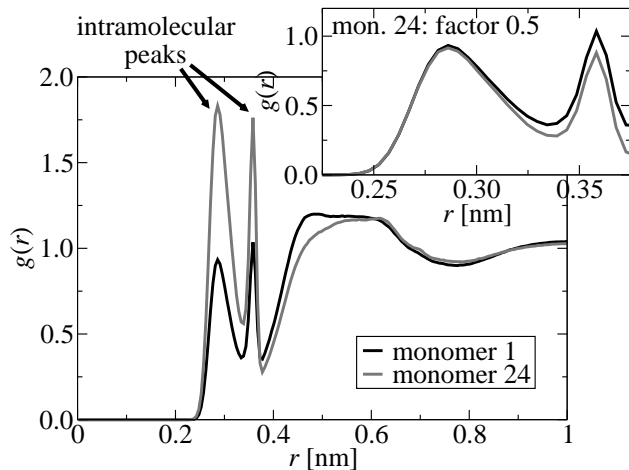


Figure 2: Radial distribution function of the terminal ($n = 1$ and $n = 48$) and the central ($n = 24$ and $n = 25$) PEO monomers in the melt. The average was performed over all chains and all initial time frames. For clarity, the curve of the central monomer has been divided by two in the inset.

Because of the additional backdragging forces, exerted by the remaining part of the polymer chain at longer times, $A_n(\Delta t)$ naturally decreases with increasing Δt . On the other hand, the dynamics in the femtosecond regime is governed by the local chemical structure and by ballistic effects. We found in our previous work¹ on the same simulation data that $A(\Delta t)$, when averaged over all monomers except the five outermost, shows quantitative agreement for the SFCM and PEO from approximately 5 ps. Due to this agreement, we will use the $A_n(\Delta t)$ -curves of the individual SFCM monomers to interpret the results for PEO.

IV. STRUCTURAL PROPERTIES

We start with the radial distribution function of the ether oxygens of the PEO chains. This quantity has been computed for both the terminal ($n = 1$ and $n = 48$) and the central ($n = 24$ and $n = 25$) PEO monomers (fig. 2). The average has been performed over all chains in the simulation box as well as over all initial time frames. Up to approximately 0.4 nm, two intramolecular peaks around $r = 0.28$ nm and $r = 0.36$ nm can be observed, corresponding to the neighbor monomer(s). The occurrence of two peaks indicates the existence of two preferred conformations (note that the root mean squared distance between the oxygen atoms of two bonded monomers is about 0.32 nm). Naturally, these peaks are approximately twice as high for $n = 24$ due to chain connectivity (see inset of fig. 2, where the curve of monomer 24 has been divided by two). When going to distances of about 0.4 – 0.5 nm, one indeed observes that the terminal monomer has more intermolecular neighbors in its first coordination shell than the central monomer.

As pointed out above, exactly these differences may alter the dynamical behavior beyond the general differences due to chain connectivity as already contained in the Rouse model.

V. DYNAMICAL PROPERTIES

In order to get a first impression of the local polymer motion, we start with the MSD, which can be regarded as a standard tool to study the dynamics in simulations.

For the MSD of the entire PEO chains, we naturally observe the well-known subdiffusive center-of-mass motion on time scales shorter than the Rouse time τ_R (not shown), which has been found in several simulations^{18–22}, experiments^{20,23} and theoretical analyses^{24,25}. It is generally believed that the subdiffusivity for realistic chains is caused by a combination of the excluded volume interactions and chain connectivity, giving rise to correlated motion of the chains²². More recently, also viscoelastic hydrodynamic interactions have been discussed²⁵ as a reason for the anomalous center-of-mass diffusion. Apart from this, we additionally observed in the present analysis that the center-of-mass diffusion is slightly anisotropic with respect to the orientation of the end-to-end vector \mathbf{R}_e in the subdiffusive short-time regime. This is demonstrated by the inset of fig. 3, which shows the ratio of the component parallel to \mathbf{R}_e relative to the total center-of-mass MSD, i. e. $\langle [(\mathbf{R}_{cm}(t + \Delta t) - \mathbf{R}_{cm}(t)) \cdot \hat{\mathbf{R}}_e(t)]^2 \rangle / \langle [\mathbf{R}_{cm}(t + \Delta t) - \mathbf{R}_{cm}(t)]^2 \rangle$. In the absence of anisotropies one would expect an ideal ratio of 1/3. However, the actual ratio is larger for all Δt shorter than the Rouse time ($\tau_R \approx 8.6$ ns for PEO), where the deviations increase until they reach a maximum at about 2 ns. This demonstrates that the preferential motion is along the primary axis of the chain, i. e. parallel to \mathbf{R}_e . A more detailed analysis reveals that both the parallel and the perpendicular component exhibit the characteristic proportionality $\langle \Delta \mathbf{R}_{cm}^2(\Delta t) \rangle \propto \Delta t^{0.8}$ until the two curves merge at about $\Delta t \approx 2\tau_R$ and cross over to diffusive behavior (not shown). In how far the observed anisotropy is related to the fact that real polymer coils are not spherical, but rather stretched in direction of \mathbf{R}_e ^{26,27} might be investigated more thoroughly in future work.

In case of the MSD of the individual monomers, one typically focuses on either the monomer-averaged MSD or, when testing the validity of specific scaling laws from e. g. the Rouse theory or the reptation model, the MSD of a few central monomers only^{5–7,21}, for which the characteristic features are most pronounced. For the monomeric MSDs, one generally observes that for intermediate time scales (i. e. $\tau_R/N^2 \leq \Delta t \leq \tau_R$) the outer monomers move faster than the central segments. Naturally, this regime is already highly affected by the connectivity constraints of the chain, which are less present for the end monomers. This is also confirmed in fig. 3, which shows the MSD of the terminal and the central PEO monomers. As stated above, the outer monomers are faster for all Δt shorter

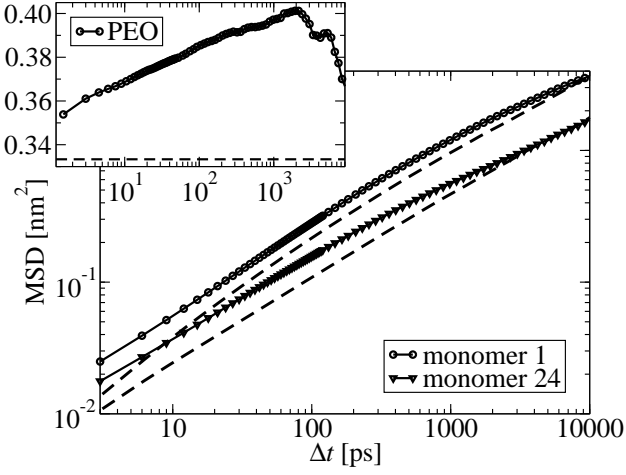


Figure 3: MSD of the terminal and the central monomers for PEO (symbols) and the SFCM (dashed line). The inset shows the ratio of the center-of-mass MSD in direction of \mathbf{R}_e and the total center-of-mass MSD for PEO. The dashed line indicates the ideal value for isotropic diffusion.

than τ_R , mainly as a result of the chain connectivity. The MSD of the respective SFCM monomers are plotted as dashed lines in fig. 3. For both the central and the outer monomers, one observes that the MSD of the SFCM is lower than the PEO curve. These deviations can be related to the more complicated local potentials for the latter system. For these reasons, it is difficult to judge whether the Rouse assumption of a uniform ζ also holds for the realistic PEO melt on the basis of the monomeric MSDs.

Alternatively, the local dynamics of the individual PEO monomers can be evaluated by the pq-method, yielding an effective mobility free from connectivity effects. Fig. 4 shows $A(\Delta t)$ for the terminal (top) and the central (bottom) PEO monomers together with the corresponding SFCM curves. For both monomer positions, one observes a good agreement of the $A(\Delta t)$ -curves of PEO (circles) and the SFCM (lines). As discussed in earlier work¹, this demonstrates that the SFCM essentially captures the local dynamical features of the PEO chains in the melt already for short time scales. This is quite remarkable, since the local potentials in PEO are much more complicated. However, the dynamical contributions arising from these potentials average out when applying the pq-method, whereas they accumulate in the MSD due to squaring (fig. 3).

In the following, we wish to investigate the directional correlations between local chain conformation and dynamics (as expressed by the correlator $\langle \mathbf{p}_n \mathbf{q}_n \rangle$ entering $A_n(\Delta t)$, see eq. 5) in more detail. Of course, even for a Rouse chain, the main dynamical contribution to the local polymer motion is oriented parallel to the contour of the chain due to the connectivity forces. In a similar spirit to the analysis presented in the inset of fig. 3, we determined the monomeric MSD parallel to the chain

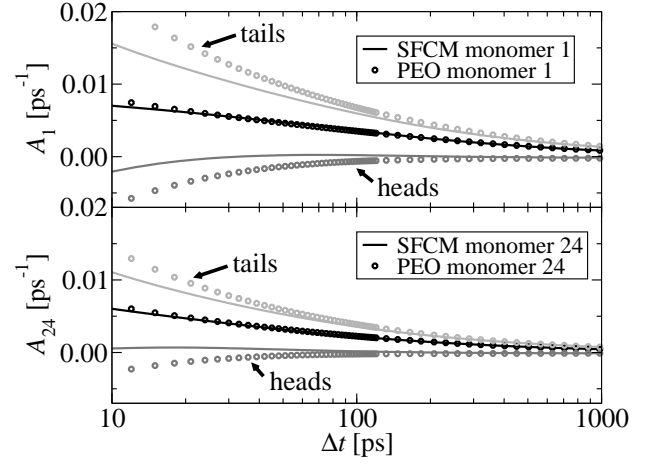


Figure 4: Effective mobilities $A_1(\Delta t)$ (top) and $A_{24}(\Delta t)$ (bottom) for the terminal and the central monomers of PEO and the SFCM. Here, a distinction was made in which direction (relative to \mathbf{q}_1 or \mathbf{q}_{24}) the center of mass of the subchain consisting of all monomers within \mathbf{q}_n moved during Δt .

contour (defined by $\mathbf{R}_1 - \mathbf{R}_5$ for the terminal and by $\mathbf{R}_{n-\Delta n} - \mathbf{R}_{n+\Delta n}$ for the inner monomers) relative to the overall MSD of the particular monomer. For both the inner and the outer monomers, we found that the relative parallel contribution is up to 6 – 8 % larger for PEO when compared to the SFCM (not shown). Obviously, the preferential motion along the contour of the chain is more pronounced for a realistic polymer chain than for a phantom chain, indicating additional correlations within one Kuhn segment beyond the trivial contributions from the chain connectivity. One would expect that the details of the restoring forces are also relevant for local relaxation measured by $A_n(\Delta t)$. In order to study the dynamical impact of these effects, we modified our analysis in the following way: For a given displacement $\Delta \mathbf{R}_{\text{cm}}^{(1-5)}(\Delta t) = \mathbf{R}_{\text{cm}}^{(1-5)}(t + \Delta t) - \mathbf{R}_{\text{cm}}^{(1-5)}(t)$ of the terminal Kuhn segment (monomers 1 – 5, center-of-mass position $\mathbf{R}_{\text{cm}}^{(1-5)}$), a distinction was made whether it moved in or against the direction of the \mathbf{q}_1 -vector. In this way, one can distinguish between head monomers ($\Delta \mathbf{R}_{\text{cm}}^{(1-5)}(\Delta t) \cdot \hat{\mathbf{q}}_1(t) > 0$), where the terminal Kuhn segment moves in front of the adjacent segments, and tail monomers ($\Delta \mathbf{R}_{\text{cm}}^{(1-5)}(\Delta t) \cdot \hat{\mathbf{q}}_1(t) < 0$), where this segment follows the local chain contour. These two contributions to $A_1(\Delta t)$ are also shown in fig. 4 (upper half). The lower half of fig. 4 shows a similar head-tail analysis for monomer 24. Here, the criterion to define head and tail monomers was if the center of mass of the subchain defined by the monomers $n - \Delta n, \dots, n + \Delta n$ moved in or against the direction of the \mathbf{q}_{24} -vector (see also sketch in fig. 1). Note that in both cases the contribution of the head monomers is partly negative, which results from their definition. Naturally, trivial head and tail contributions can also be observed for the SFCM (fig. 4) due to the bias resulting from the distinction between heads

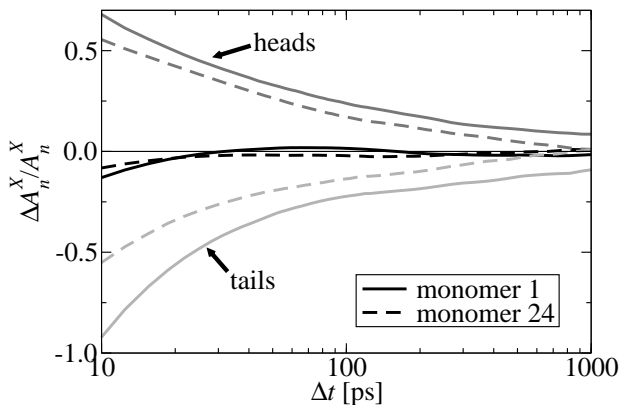


Figure 5: Relative difference between the respective SFCM and the PEO curves, defined as $\Delta A_n^X/A_n^X = (A_{\text{SFCM}}^X(\Delta t) - A_{\text{PEO}}^X(\Delta t))/A_{\text{SFCM}}^X(\Delta t)$, the index $X = \text{H}$ or T denoting head and tail monomers, respectively.

and tails. Interestingly, despite the good agreement of the average curves, the absolute values of both head and tail contributions for PEO are larger than for the SFCM. This is a consequence of the additional excluded volume, since for PEO all monomers within one Kuhn segment move much more correlated. Thus, the short-time displacement of a PEO monomer will already be dominated by the motion of the other monomers in the segment, whereas the SFCM monomers can interpenetrate each other and thus exhibit weaker motional correlations. As a result, the absolute values of $A_n^X(\Delta t)$ (with $X = \text{H}$ or $X = \text{T}$ denoting a head or a tail monomer) are larger for PEO. In a similar manner, dynamical correlations between intermolecular PEO neighbors also enhance the absolute values for $A_n^X(\Delta t)$.

In total, the additional excluded volume contributions for heads and tails approximately cancel each other for both the central as well as the terminal monomers, and the overall $A_n(\Delta t)$ -curves of PEO and the SFCM agree very well. This is also verified in fig. 5, which shows the relative differences between the respective SFCM and PEO curves, defined as $\Delta A_n^X/A_n^X = (A_{\text{SFCM}}^X(\Delta t) - A_{\text{PEO}}^X(\Delta t))/A_{\text{SFCM}}^X(\Delta t)$. The black lines correspond to the difference between the average curves, which vary within a few percent. In contrast to this, the deviations for the $A_n^X(\Delta t)$ are much more pronounced. Here, the absolute values of both $\Delta A_n^{\text{H}}/A_n^{\text{H}}$ and $\Delta A_n^{\text{T}}/A_n^{\text{T}}$ are larger for the terminal monomers, especially in case of the tail contribution. These characteristics shall be rationalized in the following. From a structural point of view, there is a fundamental difference between terminal and central monomers concerning the alignment of their \mathbf{q}_n -vector relative to the backbone of the chain: For the terminal monomers, the \mathbf{q}_1 -vector is parallel to the chain contour by definition, whereas for the inner monomers \mathbf{q}_{24} is rather perpendicular to the chain contour, especially for chains with a certain stiffness. This is also illustrated in fig. 1. Since \mathbf{q}_1 is parallel to the chain contour,

one would expect that especially the *intramolecular* excluded volume effects contribute to $A_1(\Delta t)$, whereas for $A_{24}(\Delta t)$ rather the *intermolecular* interactions are important due to the fact that \mathbf{q}_{24} is predominantly oriented perpendicular to the backbone. These details give rise to slightly different deviations of the individual PEO monomers from SFCM behavior. For the same reasons, $\Delta A_n^X/A_n^X$ for both heads and tails have a similar magnitude in case of the inner monomers, as they face basically the same intermolecular environment for either direction of motion. Contrarily, the tail deviation dominates for the peripheral monomers (fig. 5). Here, one might speculate that this residual difference is caused by the surrounding PEO chains, which occupy the newly available space whenever a terminal monomer acts as a tail and thus prevent its backward motion. Remarkably, for both the terminal and the central monomers, the detailed interplay of intra- and intermolecular effects leads to an overall cancellation of these terms, and the local PEO dynamics in the melt is essentially the same as for a phantom chain.

VI. CONCLUSION

In this contribution, we checked the fundamental Rouse assumption of a uniform friction coefficient on all monomers for a PEO melt. The mobilities were extracted from MD simulations using our previously developed pq-method¹, which avoids the classical mode picture and rather employs a Langevin-like equation to characterize the local polymer dynamics. In contrast to the MSD, this procedure leads to the cancellation of the non-trivial terms for PEO, which arise from the additional chemical potentials. In order to interpret the local PEO dynamics, we used a semiflexible phantom chain (SFCM¹⁴) as a reference.

During the course of our analysis it turned out that the effective mobility of both the terminal and the central PEO monomers is essentially the same as for the SFCM from about $\Delta t \geq 10$ ps on, the deviations being on the order of a few percent. However, this coincidental agreement results from the nearly quantitative cancellation of the more complicated interactions in the PEO melt, in particular the excluded volume effects. A more detailed analysis revealed that the relaxation with respect to the local chain curvature expressed by \mathbf{q}_n can be decomposed in two individual contributions (i. e. head and tail monomers), depending on the direction of motion of the Kuhn segment under consideration. Due to the correlated motion in PEO arising from the excluded volume interactions, both head and tail contributions are larger for PEO. However, these contributions approximately cancel, and the mobility is roughly the same for all PEO monomers.

As reported previously²⁸, our findings clearly demonstrate that the pq-method yields complementary information on the dynamics of systems involving macro-

molecules. In further work one might study in how far the chain end effects persist or enhance when approaching the glass transition temperature (cf. the Flory-Fox equation). Moreover, the pq-method is also supposed to yield fruitful results for confined polymer melts^{29,30} or complex polymer architectures³¹.

Acknowledgments

The authors would like to thank Jörg Baschnagel, Hendrik Meyer and Jean Farago for helpful discussions and

correspondence. Financial support from the NRW Graduate School of Chemistry is also greatly appreciated.

-
- * Electronic address: d.diddens@uni-muenster.de
- ¹ D. Diddens, M. Brodeck, and A. Heuer, *Europhys. Lett.* **91**, 66005 (2010).
 - ² P. E. Rouse, *J. Chem. Phys.* **21**, 1272 (1953).
 - ³ M. Doi and S. F. Edwards, *The Theory of Polymer Dynamics* (Oxford Science Publications, Clarendon, Oxford, 2003).
 - ⁴ P. G. de Gennes, *Scaling Concepts in Polymer Physics* (Cornell University Press, Ithaca, New York, 1979).
 - ⁵ K. Kremer and G. S. Grest, *J. Chem. Phys.* **92**, 5057 (1990).
 - ⁶ T. Kreer, J. Baschnagel, M. Müller, and K. Binder, *Macromolecules* **34**, 1105 (2001).
 - ⁷ W. Paul, *Chem. Phys.* **284**, 59 (2002).
 - ⁸ M. Zamponi, M. Monkenbusch, L. Willner, A. Wischniewski, B. Farago, and D. Richter, *Europhys. Lett.* **72**, 1039 (2005).
 - ⁹ T. A. Kavassalis and J. Noolandi, *Phys. Rev. Lett.* **59**, 2674 (1987).
 - ¹⁰ T. A. Kavassalis and J. Noolandi, *Macromolecules* **21**, 2869 (1988).
 - ¹¹ S. Rathgeber, L. Willner, D. Richter, A. Brulet, B. Farago, M. Appel, and G. Fleischer, *J. Chem. Phys.* **110**, 10171 (1999).
 - ¹² T. G. Fox and P. J. Flory, *J. Appl. Phys.* **21**, 581 (1950).
 - ¹³ B. Schnell, H. Meyer, C. Fond, J. P. Wittmer, and J. Baschnagel, *Eur. Phys. J. E* **34** (2011).
 - ¹⁴ R. Winkler, P. Reineker, and L. Harnau, *J. Chem. Phys.* **101**, 8119 (1994).
 - ¹⁵ A. Maitra and A. Heuer, *Macromol. Chem. Phys.* **208**, 2215 (2007).
 - ¹⁶ E. Lindahl, B. Hess, and D. van der Spoel, *J. Mol. Mod.* **7**, 306 (2001).
 - ¹⁷ O. Borodin, G. Smith, and R. Douglas, *J. Phys. Chem. B* **107**, 6824 (2003).
 - ¹⁸ W. Paul, K. Binder, D. W. Heermann, and K. Kremer, *J. Chem. Phys.* **95**, 7726 (1991).
 - ¹⁹ W. Paul, G. D. Smith, D. Y. Yoon, B. Farago, S. Rathgeber, A. Zirkel, L. Willner, and D. Richter, *Phys. Rev. Lett.* **80**, 2346 (1998).
 - ²⁰ G. Smith, W. Paul, M. Monkenbusch, and D. Richter, *Chem. Phys.* **261**, 61 (2000).
 - ²¹ W. Paul and G. Smith, *Rep. Prog. Phys.* **67**, 1117 (2004).
 - ²² J. P. Wittmer, P. Polinska, H. Meyer, J. Farago, A. Johner, J. Baschnagel, and A. Cavallo, *J. Chem. Phys.* **134** (2011).
 - ²³ M. Zamponi, A. Wischniewski, M. Monkenbusch, L. Willner, D. Richter, P. Falus, B. Farago, and M. G. Guenza, *J. Phys. Chem. B* **112**, 16220 (2008).
 - ²⁴ M. Guenza, *Phys. Rev. Lett.* **88**, 025901 (2001).
 - ²⁵ J. Farago, H. Meyer, and A. N. Semenov, *Phys. Rev. Lett.* **107** (2011).
 - ²⁶ F. Eurich and P. Maass, *J. Chem. Phys.* **114**, 7655 (2001).
 - ²⁷ C. Mischler, J. Baschnagel, and K. Binder, *Adv. Colloid Interface Sci.* **94**, 197 (2001).
 - ²⁸ D. Diddens, M. Brodeck, and A. Heuer, *Europhys. Lett.* **95**, 56003 (2011).
 - ²⁹ F. Varnik, J. Baschnagel, and K. Binder, *Phys. Rev. E* **65**, 021507 (2002).
 - ³⁰ S. Peter, H. Meyer, and J. Baschnagel, *J. Polym. Sci., Part B: Polym. Phys.* **44**, 2951 (2006).
 - ³¹ G.-L. He, H. Merlitz, J.-U. Sommer, and C.-X. Wu, *Macromolecules* **40**, 6721 (2007).

This figure "Adt_q1_q24_head_tail.png" is available in "png" format from:

<http://arxiv.org/ps/1211.3291v1>

This figure "delta_A_rel_mon1_vs_mon24.png" is available in "png" format from:

<http://arxiv.org/ps/1211.3291v1>

This figure "ev_chain_fade.png" is available in "png" format from:

<http://arxiv.org/ps/1211.3291v1>

This figure "gofr1vs24_inset.png" is available in "png" format from:

<http://arxiv.org/ps/1211.3291v1>

This figure "msd_inset_SFCM.png" is available in "png" format from:

<http://arxiv.org/ps/1211.3291v1>